Micro-kinetic modeling of NH_3 decomposition on Ni and its application to solid-oxide fuel cells

Srinivas Appari[a], Vinod M. Janardhanan[a,1], Sreenivas Jayanti[a], Steffen Tischer[b], Olaf Deutschmann[b]

[a] *Indian Institute of Technology Hyderabad, Yeddumailaram 502 205, India*
[b] *Karlsruhe Institute of Technology, Engesserstr.20, D-76131 Karlsruhe, Germany*

Abstract

This paper presents a detailed surface reaction mechanism for the decomposition of NH_3 to H_2 and N_2 on Ni surface. The mechanism is validated for temperatures ranging from 700 to 1500 K and pressures from 5.3 Pa to 100 kPa. The activation energies for various elementary steps are calculated using unity bond index-quadratic exponential potential (UBI-QEP) method. Sensitivity analysis is carried out to study the influence of various kinetic parameters on reaction rates. The NH_3 decomposition mechanism is used to simulate SOFC button cell operating on NH_3 fuel.

Key words:
NH_3 decomposition, Catalysis, Kinetics, SOFC ,Mathematical modelling,Reaction engineering

Introduction

A practical alternative to challenges of H_2 storage for portable and decentralized power generation is to produce it on site from hydrides. Ammonia (NH_3) is considered as a perfect H_2 carrier and has a worldwide distribution infrastructure (Christensen et al., 2006). Recently NH_3 started gaining attention as a source of H_2 for fuel cell applications (Kaisare et al., 2009, Li and Hurley, 2007). The major draw back of NH_3 is its toxicity which imposes stringent regulations on its emission. Otherwise NH_3 has the advantageous over alcohols and hydrocarbon fuels that it is CO free, and therefore a good source of H_2 for polymer electrolyte membrane fuel cells (PEMFC). However, it may be used directly in solid-oxide fuel cells (SOFC) without upstream fuel processing (Fuerte et al., 2009). Motivated by application of NH_3 as a fuel for SOFCs and a source of H_2 for PEMFC, this paper presents a detailed kinetic model for the decomposition of NH_3 on Ni.

There are many studies on direct NH_3 solid oxide fuel cells; some of them are on proton conductnig systems (SOFC-H) (Ma et al., 2006b,a, Maffei et al., 2006, 2005, 2008, Ni et al., 2008, Zhang and Yang, 2008), and others are on oxygen ion conducting systems (SOFC-O) (Fournier et al., 2006, Fuerte et al., 2009, Ma et al., 2007, Meng et al., 2007). Based on open circuit potential analysis Fuerte et al. concluded that NH_3 oxidation is a two stage process in SOFC; decomposition of NH_3 into H_2 and N_2 and then the electrochemical oxidation of H_2 to H_2O (Fuerte et al., 2009).

Decomposition of NH_3 is a mildly exothermic reaction ($\Delta_R H = 45.9$ kJ/mol), and can be achieved catalytically over Pt, Pd, Rh, Ni, Ru etc. (Papapolymerou and Bontozoglou, 1997, Löffler and Schmidt, 1976, Choudhary et al., 2001, Zheng et al., 2007). There are many studies on NH_3 decomposition over supported metal catalysts. Choudary et al. systematically studied NH_3 decomposition on Ni, Ir, and Ru catalyst. They found Ni to be less active compared to Ir and Ru. Moreover, their study shows that the catalyst support does play a role in the overall catalytic activity (Choudhary et al., 2001). Most of the NH_3 decomposition studies are carried out at very low pressures. For instance Löffer and Schimidt studied the kinetics of NH_3 decomposition over Pt catalysts and developed a Langmuir-Hinshelwood rate expression which fitted their experimental measurements (Löffler and Schmidt, 1976). However, the experiments were carried out for pressure ranges of 0.01 to 1.25 Torr.

Choudary et al. studied the decomposition of NH_3 on supported metal catalysts at high pressures and temperature and concluded that Ru is a better catalyst compared to Ni and Ir (Choudhary et al., 2001). In another significant work McCabe studied the kinetics of NH_3 decomposition over Ni wires at high temperatures and low pressures (McCabe, 1983). These two works serves to validate the model developed in this work.

Kinetic model

The mechanism of NH_3 decomposition has been assumed to consists of the following steps

$$H_{2,g} \rightleftarrows H_{2,s} \rightleftarrows 2H_s, \quad (1)$$

$$N_{2,g} \rightleftarrows N_{2,s} \rightleftarrows 2N_s, \quad (2)$$

$$NH_{3,g} \rightleftarrows NH_{3,s}, \quad (3)$$

Email address: vj@iith.ac.in (Vinod M. Janardhanan)

$$NH_{3,s} \rightleftarrows NH_{2,s} + H_s, \quad (4)$$

$$NH_{2,s} \rightleftarrows NH_s + H_s, \quad (5)$$

$$NH_s \rightleftarrows N_s + H_s. \quad (6)$$

Based on the above mechanism the detailed kinetic model presented here is developed based on unity bond index-quadratic exponential potential (UBI-QEP) method (Shustorovich, 1990). This phenomenological method treats the energetics of atomic and polyatomic adsorbates on transition metal surfaces by using the chemisorption and bond dissociation energies. Therefore, the input data required for the model development are the chemisorption energy and the gas-phase dissociation energy.

Closed shell molecules such as NH_3 establishes a weak bonding with the metal atom and for such cases the chemisorption energy is calculated according to Eq. 7 (Shustorovich and Bell, 2001)

$$Q_{AB} = \frac{Q_{0A}^2}{(Q_{0A}/n) + D_{AB}}. \quad (7)$$

Here Q_{0A} corresponds to the maximum M-A two center bond energy (Shustorovich, 1990). For an ad-atom in an *n*-fold site the maximum two center bond energy is given by

$$Q_A = Q_{0A}(2 - 1/n), \quad (8)$$

where n is the number of nearest metal atoms. For strongly bonded radicals such as NH and NH_2 the chemisorption energy is calculated according to

$$Q_{AB} = \frac{Q_A^2}{Q_A + D_{AB}}. \quad (9)$$

Based on Eq. 7 we determined the chemisorption energy of NH_3 on Ni to be 18 kcal/mol, which is in good agreement with experimental (20 kcal/mol) and Ab initio calculation (17-19 kcal/mol) reported respectively by Klauber et al. and Chattopadhyay et al. (Klauber et al., 1985, Chattopadhyay et al., 1990). The calculated chemisorption energy for NH, NH_2 and NH_3 is given in Table 1.

The mechanism of NH_3 decomposition involves the adsorption of NH_3 from the gas-phase on to the Ni surface (Eq. 3) and the subsequent hydrogen abstraction steps given by Eqs. 4, 5, and 6. The hydrogen and nitrogen atoms recombine to form gas-phase hydrogen and nitrogen (Eqs. 1 and 2).

Once the chemisorption and dissociation energies of all chemical species are known the activation energy barriers for various adsorption, desorption, and recombination steps can be evaluated from general thermodynamic relationships. However, in the following treatment, we assign sticking coefficient for adsorption reactions. The sticking coefficient for NH_3 is taken from McCabe (McCabe, 1983). For recombination of chemisorbed A_s and B_s to chemisorbed AB_s or for the associative desorption of chemisorbed A_s and B_s to AB_g the activation barriers $\Delta E^*_{A-B,s}$ and $\Delta E^*_{A-B,g}$ may be same or different depending on the sign of gasphase dissociation barrier (Shustorovich, 1990). i.e,

$$\Delta E^*_{A-B,s} = \Delta E^*_{A-B,g} = Q_A + Q_B - D_{AB} + \Delta E^*_{AB,g} \quad \text{if} \quad \Delta E^*_{AB,g} > 0, \quad (10)$$

and

$$\Delta E^*_{A-B,g} = \Delta E^*_{A-B,s} - \Delta E^*_{AB,g} = Q_A + Q_B - D_{AB} \quad \text{if} \quad \Delta E^*_{AB,g} > 0. \quad (11)$$

The gasphase dissociation barrier $\Delta E^*_{AB,g}$ can be evaluated according to

$$\Delta E^*_{AB,g} = 1/2\left(D_{AB} + \frac{Q_A Q_B}{Q_A + Q_B} - Q_{AB} - Q_A - Q_B\right) \quad (12)$$

The detailed surface reaction mechanism developed here consists of two parts. The first part deals with the catalytic decomposition of NH_3, which has 12 reactions among three gas-phase species and five surface adsorbed species. In the second part additional reactions for H_2 oxidation is considered so that the mechanism can be used for direct NH_3 SOFC as well. The reactions in the second part are taken from Janardhanan and Deutschmann (Janardhanan and Deutschmann, 2006). The complete mechanism is listed in Table 2. Reactions R1 to R12 are steps for the decomposition of NH_3 on Ni surface and reactions from R13 to R22 are for hydrogen oxidation on Ni. One needs to consider all the reactions for direct NH_3 SOFC, while reactions from R1 to R12 are sufficient to study NH_3 decomposition on Ni. There are slight variations in the rate parameters for R13 to R22 as reported against Janardhanan et al. (Janardhanan and Deutschmann, 2006). These slight variations are made to ensure that the entire mechanism is thermodynamically consistent. The thermodynamic consistency is explained in the following section.

The net molar production rate $\dot{s}_k$ of a gaseous or surface adsorbed species due to heterogeneous reaction is given by

$$\dot{s}_k = \sum_{i=1}^{R_s} \nu_{ki} k_{fi} \prod_{k=1}^{N_g+N_s} [X_k]^{\nu''_{ki}}. \quad (13)$$

Here R_s is the number of surface reactions, N_g and N_s respectively represents the number of gasphase species and surface species, $[X_k]$ is the concentration of species k, k_{fi} is the forward rate constant for reaction i, and ν_{ki} is the difference in stoichiometric coefficient for species k between the products and reactants in reaction i.

Based on mean field approximation the forward rate constant is expressed in the Arrhenius form as

$$k_{fi} = A_i T^\beta \exp\left(-\frac{E_{ai}}{RT}\right) \prod_{k=1}^{K_s} \theta_k^{\mu_{ki}} \exp\left(-\frac{\epsilon_{ki}\theta_k}{RT}\right) \quad (14)$$

Here A_i is the pre-exponential factor and E_{ai} is the activation energy, μ is the order dependency, θ is the surface coverage, β

is the temperature exponent, R the gas constant, T the temperature, and ϵ is the coverage dependent activation energy.

Thermodynamic consistency

The equilibrium of a chemical reaction

$$\sum_k \nu'_{ki} A_k \rightleftarrows \sum_k \nu''_{ki} A_k, \tag{15}$$

is completely defined by the thermodynamic properties of the participating species. Expressed in terms of the equilibrium constant K_{pi}, the equilibrium activities a_k^{eq} obey the equation

$$K_{pi} = \prod_k \left(a_k^{\mathrm{eq}}\right)^{\nu_{ki}} = \exp\left(-\frac{\Delta_i G^0}{RT}\right). \tag{16}$$

Here R is the gas constant and T is the absolute temperature. The change of free enthalpy ΔG^0 at normal pressure p^0 is given by

$$\Delta_i G^0 = \sum_k \nu_{ik} G_k^0(T). \tag{17}$$

When the heat capacity is expressed as a forth order polynomial function of temperature T, then the standard free enthalpies can be expressed in terms of seven coefficients, $a_{0,\mathrm{i}} \ldots a_{6,\mathrm{i}}$ as

$$G_k^0 = a_{0,\mathrm{k}} + a_{1,\mathrm{k}} T + a_{2,\mathrm{k}} T^2 + a_{3,\mathrm{k}} T^3 + a_{4,\mathrm{k}} T^4 + a_{5,\mathrm{k}} T^5 + a_{6,\mathrm{k}} T \ln T \tag{18}$$

In order to predict the correct equilibrium, the rate coefficients for forward and the reverse reaction must obey the equation

$$\frac{k_{fi}}{k_{ri}} = K_{\mathrm{pi}} \prod_k (c_k^0)^{\nu_{ki}} \tag{19}$$

c_k^0 are the reference concentrations at normal pressure, i.e, $c_k^0 = p^0/RT$ for gas-phase species and $c_k^0 = \Gamma/\sigma_k$ for surface species; here Γ is the total surface site density and σ_k are the site occupancy number for species k. However, one problem in setting up a reaction mechanism is the difficulty to define the thermo-chemistry data for intermediate species. Therefore, when the thermo-chemistry data for the intermediate species are unknown Eq. 19 can not be used to calculate the reverse reaction rate constants. The forward and reverse reaction rates are then defined separately with their own rate laws. Nevertheless, these rates cannot be chosen independently.

Assuming an initial guess for the rate parameters of a surface reaction mechanism, the rate coefficient for the forward and reverse reactions may be adjusted separately to make the entire mechanism thermodynamically consistent. Suppose that the thermodynamic data for species $1 \ldots N_{\mathrm{u}}$ out of N species are unknown. For each pair of a reversible reactions we can calculate the equilibrium constant according to Eq. 19 and, logarithm of Eq. 16 yields change of free enthalpy. Separation of the known and unknown variables in Eq. 17 leads to

$$\Delta_i G^0 = \sum_{k=1}^{N_{\mathrm{u}}} \nu_{ki} \tilde{G}_k^0(T) + \sum_{k=1+N_{\mathrm{u}}}^{N} \nu_{ki} G_k^0(T), \tag{20}$$

which is a linear equation system for the unknown free enthalpies $\tilde{G}_k^0$. Since most species are involved in more than one reaction, this system is usually over-determined. Equation 18 for several temperatures T_j gives a system of linear equations in the unknown coefficients $\tilde{a_{l,k}}$:

$$\sum_{k=1}^{N_{\mathrm{u}}} \sum_{l=0}^{6} \nu_{ki} t_{lj} \tilde{a_{l,j}} = g_{ij}, \tag{21}$$

here

$$g_{ij} = \Delta_i G^0(T_j) - \sum_{k=N_u+1}^{N} \nu_{ki} G_k^0(T_j) \tag{22}$$

and

$$t_{lj} = \begin{cases} T_j^l & \texttt{if} \quad l < 6 \\ T_j \ln T_j & \texttt{if} \quad l = 6 \end{cases} \tag{23}$$

An optimal set of parameters $\tilde{a_{l,k}}$ is determined by a weighted least-square approximation. The weights can be chosen individually for each pair of reactions according to a sensitivity analysis of the reaction mechanism. This guarantees that the equilibrium of crucial reaction steps will be shifted less then others after the adjustment.

The newly adjusted polynomial coefficients are then used to calculate the change of free enthalpy for each reaction (Eq. 20), the equilibrium constant, and the rate coefficient for the reverse reaction. In case the reverse reaction shall be expressed in terms of Arrhenius coefficients, another least square approximation using the rate constants at the discrete temperatures, T_j is performed.

Since we prefer to write surface reaction mechanisms as pairs of irreversible reactions, this procedure has to be repeated during mechanism development after modification of rate coefficients belonging to any of these pairs. The difference between this method and the scheme proposed by Mhadeshwar et al. (Mhadeshwar et al., 2003) is that there is no need for the user to select a linearly independent set of reactions. Instead of distinguishing reactions between linear base and linear combinations, all reactions are treated equally by solving the same linear problem using a least-square fit.

Reactor model

A packed bed reactor model is used to validate the reaction mechanism. An isothermal packed bed reactor model is implemented in FORTRAN assuming

- axial diffusion of any quantity is negligible compared to corresponding convective term.
- there are no variations in the transverse direction.

The species transport equation in one dimension is modeled as

$$\frac{d(\rho u Y_k)}{dz} = a_v W_k \dot{s_k}. \tag{24}$$

Here a_v is the specific area of the catalyst and W_k is the molecular weight of the species k. Summing the species transport equation over all species N_g leads to the total continuity equation as

$$\frac{d(\rho u)}{dz} = a_v \sum_{k=1}^{N_g} W_i \dot{s}_k. \tag{25}$$

The pressure in the reactor is calculated according to

$$\frac{dp}{dz} = f\frac{\rho u^2}{d_p}, \tag{26}$$

and density is calculated from ideal gas equation

$$\rho = \frac{P\bar{M}}{RT}. \tag{27}$$

The friction factor f in Eq. 26 is calculated from Ergun's equation as

$$f = \frac{1-\epsilon}{2\epsilon^3}\left[1.75 + \frac{150(1-\epsilon)}{Re}\right], \tag{28}$$

where Re is the Reynolds number and ϵ is the porosity. The packed bed reactor model is a part of DETCHEM software (Deutschmann et al., 2007).

Fuel cell model

A detailed description of the SOFC model used in this work is published elsewhere (Zhu et al., 2005). However, the electrochemistry model is implemented differently. Instead of using the modified Butler-Volmer equation, we implement the Butler-Volmer equation in the conventional form as

$$i = i_a^0\left[\exp\left(\frac{\alpha_a n_e F \eta_a}{RT}\right) - \exp\left(\frac{(1-\alpha_a) n_e F \eta_a}{RT}\right)\right], \tag{29}$$

and

$$i = i_c^0\left[\exp\left(\frac{\alpha_c n_e F \eta_c}{RT}\right) - \exp\left(\frac{(1-\alpha_c) n_e F \eta_c}{RT}\right)\right]. \tag{30}$$

Here α_a and α_c are respectively the asymmetry factors for anode and cathode side, F is the Faraday constant, R the gas constant, T the temperature, and n_e is the number of electrons transferred. The exchange current densities for the anode side and cathode side i_a^0 and i_c^0 are functions of temperature and concentration. However, in the present work we consider them to be only as a function of temperature. i.e,

$$i_a^0 = k_{H_2} \exp(-E_{H_2}/RT), \tag{31}$$

and

$$i_c^0 = k_{O_2} \exp(-E_{O_2}/RT), \tag{32}$$

Since the species transport equation considers the porous media transport, concentration losses are not treated explicitly. The activation losses of the anode and cathode sides are related to the cell potential as

$$E_{\text{cell}} = E_{\text{rev}} - \eta_a - \eta_c - \eta_{\text{ohm}}. \tag{33}$$

The ohmic overpotential is calculated according to

$$\eta_{\text{ohm}} = L_{\text{el}}/\sigma_{\text{el}}, \tag{34}$$

where L is the length of the electrolyte and σ is the conductivity defined as

$$\sigma_{\text{el}} = \sigma_0 T^{-1} \exp\left(-\frac{E_{\text{el}}}{RT}\right). \tag{35}$$

Results and discussion

Mechanism validation

Thermodynamic analysis of NH_3 + O_2 system shows that at temperatures below 1000 K (typical operating temperature for direct NH_3 SOFC) the amount of NO_x formed is very much negligible. Six gas-phase species namely NH_3, O_2, H_2, H_2O, NO, and NO_2 are considered for thermodynamic equilibrium calculations. Figures 1 and 2 shows the map of NO and NO_2 mole fraction as a function of temperature for an initial mixture of O_2 and NH_3. In these figures as the mole fraction of O_2 increases from 0 to 1, the mole fraction of NH_3 decreases from 1 to 0. Composition of NO_2 is maximum at 1500 K for O_2:NH_3 ratio of 0.2:0.8. However, for NO the O_2:NH_3 ratio is 0.4:0.6. The experiments performed by Ma et al. also reports the absence of NO at the anode exhaust (Ma et al., 2006b). Furthermore, the partial pressure of oxygen, which results from the dissociative desorption of H_2O in the anode compartment of an SOFC will be much lower than that required for NO_x formation. Therefore, in the present mechanism reaction steps leading to the formation of NO_x are not considered.

Although there are numerous studies on catalytic decomposition of NH_3, there are no consensus on the rate limiting steps of NH_3 decomposition on different catalysts under different operating conditions (Ni et al., 2009). For model validation purpose we consider the data reported by McCabe and Choudary et al., (McCabe, 1983, Choudhary et al., 2001).

Choudary et al. studied the decomposition of NH_3 decomposition on various supported metal catalysts. A 2 cm long packed bed reactor is used for simulating the experiments reported by Choudary et al., (Choudhary et al., 2001). The geometrical parameters of the reactor and the operating conditions are listed in Table 3 and the reactor model itself is presented in one of the previous sections. A comparison between experimentally observed conversion of NH_3 for Ni supported on SiO_2 and the model predictions at 1 atm is shown in Fig. 3. Very good agreement is observed between the model predictions and the measured values. McCabe carried out NH_3 decomposition experiments over resistive heated wires at pressures between 5.3 and 133 Pa and temperatures between 700 and 1400 K (McCabe, 1983). A comparison between the experimentally measured rate and the mechanism predicted rate for the decomposition of NH_3 for the data reported by McCabe is shown in Fig. 4. Again very good agreement is observed between the model predictions and the experimental observations at temperatures above 1000 K for all pressures.

Sensitivity analysis

Sensitivity analysis for the NH_3 decomposition part of the mechanism is carried out by changing the pre-exponential factor (A) of each reaction by ±10%, while keeping all other operating parameters constant. The scaled sensitivity coefficient (SSC) for NH_3 conversion is defined as (Mantri and Aghalayam, 2007)

$$\mathrm{SSC} = \frac{X_{\mathrm{NH_3}} - X^0_{\mathrm{NH_3}}}{X^0_{\mathrm{NH_3}}}. \tag{36}$$

Here $X_{\mathrm{NH_3}}$ indicates NH_3 conversion for ±10% change in pre-exponential factors and $X^0_{\mathrm{NH_3}}$ indicates the conversions for the pre-exponential factors as noted in Table 2. These sensitivity coefficients are further normalized with respect to the maximum SSC. A plug flow reactor model is used for sensitivity analysis. 100% NH_3 is assumed to enter reactor at a velocity of 10 cm/s and 1 atm pressure. The catalytic area to geometric area factor of 100 is chosen so that ~99% NH_3 conversion is obtained for the parameters given in Table 2. The catalytic area to geometric area is a measure of catalyst loading and a higher factor indicates higher catalyst loading (Mladenov et al., 2010). Figure 5 shows the normalized sensitivity coefficient (NSC) for NH_3 conversion. Small values of NSC indicates that particular reaction has no significant effect on NH_3 conversion. It is quite obvious from the figure that the sticking coefficient of N_2 (R3) does not have any influence on NH_3 conversion, where as decreasing H_2 sticking coefficient and increasing NH_3 sticking coefficient has positive effect on NH_3 conversion. Among the sticking reactions, the sticking coefficient of NH_3 has highest influence on NH_3 conversion. Other than sticking reactions, hydrogen abstraction from surface adsorbed NH_3 (R7) and NH_2 (R9) are the most influential reactions. NH_3 conversion is least affected by the rate constants of reactions R10, R11 and R12.

SOFC modeling

Ma et al. have reported performance of a conventional SOFC button cell (Ni-YSZ/YSZ/LSM-YSZ) at different temperatures using H_2 as well as NH_3 fuel (Ma et al., 2007). The micro-kinetic model developed here is used to simulate the experiments and the results are shown in Fig. 6. For carrying out these simulations, we assume H_2 as the only electrochemically active species and the electrochemical model parameters are fixed by reproducing the experimental observation for H_2 fuel, and the same parameters are applied for NH_3 fuel. Figure 6(a) shows the comparison between model predictions and experimental observation for H_2 fuel. The model parameters are given in Table. 4. The comparison between the experimental observations and the model predictions for NH_3 fuel is shown in Fig. 6(b). Overall, good agreement is observed between the measured values and the model predictions. Under identical conditions the model predicts similar performances for both H_2 and NH_3, which is in very good agreement with experimental observations. NH_3 which enters the anode compartment decomposes into H_2 and N_2, and H_2 further participates in the charge transfer reactions. The comparable performance of NH_3 with H_2 indicates that significant conversion of NH_3 occurs in the anode and the presence of N_2 as a diluent does not affect the cell performance adversely. This is again confirmed by running the model with 75% H_2 and 25% N_2, which gave performance curves very close to that of 99% H_2 under identical operating conditions.

A comparison of kinetically predicted limiting current for button cell as a function of specific surface area is shown in Fig. 7. As the surface area increases, the limiting current approaches the equilibrium predictions. The equilibrium prediction is calculated by considering 75% H_2 and 25% N_2.

The kinetics model can be quite useful when planar or tubular cell calculations are desired. The species molefractions and the current density for a 10 cm long planar cell is shown in Fig. 8. The channel is modeled under isothermal condition of 1023 K with the same membrane electrode assembly parameters as given in table 4. 100% NH_3 is considered to enter the cell at a velocity of 0.1 m/s. NH_3 is fully converted within 2 cm from the cell inlet. Although no H_2 is present in the inlet fuel, H_2 is generated within the porous media by catalytic decomposition of NH_3. The H_2 thus generated takes part in the electrochemical charge transfer reactions occuring at the anode electrolyte interface. The current density drops along the length of the channel because of H_2 depletion.

Conclusions

We have developed a micro-kinetic model for the decomposition of NH_3 on Ni catalyst. The decomposition mechanism is supplemented with H_2 oxidations reactions reported previously so that the model can be used for direct NH_3 SOFC. Furthermore, the overall mechanism is made thermodynamically consistent in enthalpy as well as in entropy. The decomposition mechanism is validated by comparing against experimental observations over a wide range of temperatures and pressures. The complete mechanism is used to model the direct NH_3 SOFC experiments reported by Ma et al., (Ma et al., 2007). Overall the model predictions are in very good agreement with experimental observations.

References

Chattopadhyay, A., Yang, H., Whitten, J. L., 1990. Ammonia on Ni(111). J. Phys. Chem. 94 (28), 6379–6383.

Choudhary, T. V., Sivadinarayana, C., Goodman, D. W., 2001. Catalytic ammonia decomposition : CO_x -free hydrogen production for fuel cell applications. Catal. Lett. 72 (3), 197–201.

Christensen, C. H., Johannessen, T., Sorensen, R. Z., Noroskov, J. K., 2006. Towards an ammonia-mediated hydrogen economy ? Catal. Today 111, 140–144.

Deutschmann, O., Tischer, S., Kleditzsch, S., Janardhanan, V. M., Mladenov, N., Minh, H. D., 2007. DETCHEM User manual.
URL `www.detchem.com`

Fournier, G., Cumming, I., Hellgardt, K., Nov. 2006. High performance direct ammonia solid oxide fuel cell. Journal of Power Sources 162 (1), 198–206.

Fuerte, A., Valenzuela, R., Escudero, M., Daza, L., Jul. 2009. Ammonia as efficient fuel for SOFC. Journal of Power Sources 192 (1), 170–174.

Janardhanan, V. M., Deutschmann, O., 2006. CFD analysis of a solid oxide fuel cell with internal reforming : Coupled interactions of transport , heterogeneous catalysis and electrochemical processes. J. Power Sources 162, 1192–1202.

Kaisare, N. S., Stefanidis, G. D., Vlachos, D. G., 2009. Millisecond Production of Hydrogen from Alternative, High Hydrogen Density Fuels in a Cocurrent Multifunctional Microreactor. Ind. Eng. Chem. Res. 48, 1749–1760.

Klauber, C., Alvey, M. D., Yates, J. T., J., 1985. NH_3 adsorption on Ni(110) and the production of the NH_2 species by electron irradiation. Surf. Sci. 154, 139–167.

Li, L., Hurley, J., Jan. 2007. Ammonia-based hydrogen source for fuel cell applications. International Journal of Hydrogen Energy 32 (1), 6–10.

Löffler, D. G., Schmidt, L. D., 1976. Kinetics of NH_3 , decomposition on single crystal planes of Pt *. Surf. Sci. 59 (March), 195–204.

Ma, Q., Ma, J., Zhou, S., Yan, R., Gao, J., Meng, G., Jan. 2007. A high-performance ammonia-fueled SOFC based on a YSZ thin-film electrolyte. J. Power Sources 164 (1), 86–89.

Ma, Q., Peng, R., Lin, Y., Gao, J., Meng, G., Oct. 2006a. A high-performance ammonia-fueled solid oxide fuel cell. J. Power Sources 161 (1), 95–98.

Ma, Q., Peng, R., Tian, L., Meng, G., Nov. 2006b. Direct utilization of ammonia in intermediate-temperature solid oxide fuel cells. Electrochem. Commun. 8 (11), 1791–1795.

Maffei, N., Pelletier, L., Charland, J., Mcfarlan, A., Feb. 2005. An intermediate temperature direct ammonia fuel cell using a proton conducting electrolyte. J. Power Sources 140 (2), 264–267.

Maffei, N., Pelletier, L., Charland, J., Mcfarlan, A., Nov. 2006. An ammonia fuel cell using a mixed ionic and electronic conducting electrolyte. J. Power Sources 162 (1), 165–167.

Maffei, N., Pelletier, L., Mcfarlan, A., Jan. 2008. A high performance direct ammonia fuel cell using a mixed ionic and electronic conducting anode. J. Power Sources 175 (1), 221–225.

Mantri, D., Aghalayam, P., 2007. Detailed surface reaction mechanism for reduction of NO by CO. Catal. Today 119, 88–93.

McCabe, R., Feb. 1983. Kinetics of ammonia decomposition on nickel. J. Catal. 79 (2), 445–450.

Meng, G., Jiang, C., Ma, J., Ma, Q., Liu, X., Nov. 2007. Comparative study on the performance of a SDC-based SOFC fueled by ammonia and hydrogen. J. Power Sources 173 (1), 189–193.

Mhadeshwar, A. B., Wang, H., Vlachos, D. G., 2003. Thermodynamic Consistency in Microkinetic Development of Surface Reaction Mechanisms. J. Phys. Chem. B 107 (46), 12721–12733.

Mladenov, N., Koop, J., Tischer, S., Deutschmann, O., 2010. Modeling of transport and chemistry in channel flows of automotive catalytic converters. Chem. Eng. Sci. 65, 812–826.

Ni, M., Leung, D., Leung, M., Oct. 2008. An improved electrochemical model for the NH3 fed proton conducting solid oxide fuel cells at intermediate temperatures. J. Power Sources 185 (1), 233–240.

Ni, M., Leung, M. K. H., Leung, D. Y. C., 2009. Ammonia-fed solid oxide fuel cells for power generation A review. Int. J. Energy Res. 33 (June), 943–959.

Papapolymerou, G., Bontozoglou, V., 1997. Decomposition of NH_3 , on Pd and Ir Comparison with Pt and Rh. J. Mol. Catal. A: Chem. 120, 165–171.

Shustorovich, E., 1990. The bond-order conservation approach to chemisorption and heterogeneous catalysis: Applications and implications.

Shustorovich, E., Bell, A. T., 2001. Synthesis and decomposition of ammonia on transition metal surfaces : bond-order-conservation-Morse-potential analysis. Surf. Sci. Lett 259 (1991), L791–L796.

Zhang, L., Yang, W., Apr. 2008. Direct ammonia solid oxide fuel cell based on thin proton-conducting electrolyte. J. Power Sources 179 (1), 92–95.

Zheng, W., Zhang, J., Xu, H., Li, W., Aug. 2007. NH3 Decomposition Kinetics on Supported Ru Clusters: Morphology and Particle Size Effect. Catal Lett 119 (3-4), 311–318.

Zhu, H., Kee, R. J., Janardhanan, V. M., Deutschmann, O., Goodwin, D. G., 2005. Modeling Elementary Heterogeneous Chemistry and Electrochemistry in Solid-Oxide Fuel Cells. J. Electrochem. Soc. 152, A2427–A2440.

Table 1: Heats of chemisorption and total bond energies in the gas phase (D) and chemisorbed (D+Q) states on Ni(111)

Adsorbate	D	Q	$D+Q$
H	-	63	63
N	-	135	135
NH	81	85[a]	166
NH_2	169	60[a]	229
NH_3	279	18[b]	323

All energies are in kcal/mol
[a]calculated according to Eq. 9
[b]calculated according to Eq. 7

Table 2: Detailed kinetic model for NH_3 decomposition for SOFC applications

R No	Reaction	A(cm,mol,s)	β	E_a[a]
	NH_3 decomposition			
R1	H_2 + (Ni) + (Ni) → H(Ni) + H(Ni)	0.01 [b]	0	0
R2	NH_3 + (Ni) → NH_3(Ni)	0.011[b]	0	0
R3	N_2 + (Ni) + (Ni) → N(Ni) + N(Ni)	1.000×10^{-06}[b]	0	0
R4	H(Ni) + H(Ni) → H_2 + (Ni) + (Ni)	3.315×10^{19}	0	82.21
R5	NH_3(Ni) → NH_3 + (Ni)	8.210×10^{14}	0	78.63
R6	N(Ni) + N(Ni) → N_2 + (Ni) + (Ni)	4.442×10^{22}	0	210.84
R7	NH_3(Ni) + (Ni) → NH_2(Ni) + H(Ni)	5.723×10^{22}	0	78.99
R8	NH_2(Ni) + H(Ni) → NH_3(Ni) + (Ni)	1.320×10^{24}	0	48.81
R9	NH_2(Ni) + (Ni) → NH(Ni) + H(Ni)	2.718×10^{22}	0	75.74
R10	NH(Ni) + H(Ni) → NH_2(Ni) + (Ni)	3.702×10^{19}	0	74.87
R11	NH(Ni) + (Ni) → N(Ni) + H(Ni)	6.213×10^{19}	0	22.93
R12	N(Ni) + H(Ni) → NH(Ni) + (Ni)	2.070×10^{19}	0	156.04
	*H_2 oxidation*Janardhanan and Deutschmann (2006)			
R13	O_2 + (Ni) +(Ni) → O(Ni) + O(Ni)	0.01[b]	0	0
R14	O(Ni) + O(Ni) → O_2 + (Ni) +(Ni)	3.928×10^{23}	0	473.41
R15	H_2O + (Ni) → H_2O(Ni)	0.1[b]	0	0
R16	H_2O(Ni) → (Ni) + H_2O	4.747×1^{12}	0	62.09
R17	O(Ni) + H(Ni) → OH(Ni) + (Ni)	5.00×10^{22}	0	97.90
R18	OH(Ni) + (Ni) → O(Ni) + H(Ni)	1.761×10^{21}	0	36.00
R19	OH(Ni) + H(Ni) → H_2O(Ni) + (Ni)	3.000×10^{20}	0	42.70
R20	H_2O(Ni) + (Ni) → OH(Ni) + H(Ni)	2.068×10^{21}	0	91.07
R21	OH(Ni) + OH(Ni) → O(Ni) + H_2O(Ni)	3.000×10^{21}	0	100.00
R22	O(Ni) + H_2O(Ni) → OH(NI) + OH(Ni)	5.871×10^{23}	0	210.27

[a]Arrhenius parameters for the rate constants written in the form: $k = AT^{\beta} \exp(E/RT)$. The units of A are given in terms of moles, centimeters, and seconds. E is in kJ/mol
[b]Sticking coefficient. Total available surface site density is $\Gamma=2.49\times10^{-9}$ mol/cm^2

Table 3: Packed bed reactor parameters

Parameters	value
Length (cm)	2
Diameter (mm)	10
Particle diameter (μm)	20
Porosity	38%
Specific area (1/m)	2.8×10^5
Inlet conditions	
Inlet velocity (m/s)	0.1
NH_3 mole fraction	1.0

Table 4: SOFC button cell membrane electrode assembly (MEA) parameters

Parameters	value	units
Anode		
Thickness	500	μm
Porosity	45%	
Tortuosity	3.8	
Pore diameter	1.0	μm
Particle diameter	1.0	μm
Specific area	2025×10^{3}	1/m
Prefactor for exchange current density (k_{H_2})	1.87×10^{3}	A/cm^2
Activation energy for exchange current density (E_{H_2})	81.6	kJ/mol K
Symmetry factor (α_a)	0.36	
Cathode		
Thickness	8	μm
Porosity	45%	
Tortuosity	3.8	
Pore diameter	1.0	μm
Particle diameter	1.0	μm
Prefactor for exchange current density (k_{H_2})	27.7	A/cm^2
Activation energy for exchange current density (E_{H_2})	45.3	kJ/mol K
Symmetry factor (α_c)	0.35	
Electrolyte $\sigma_{el} = \sigma_0 T^{-1} \exp(-E_{el}/RT)$		
Thickness	10	μm
Activation energy (E_{el})	80	kJ/mol
Pre-factor (σ_0)	3.6×10^{5}	S/cm

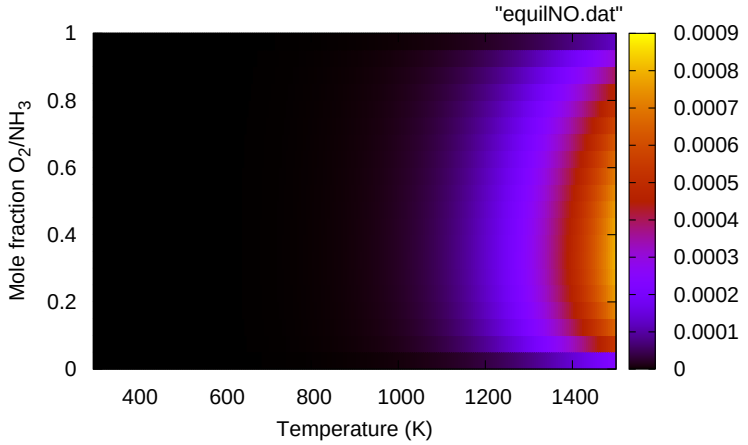

Figure 1: Map of equilibrium composition of NO resulting from a mixture of O_2 and NH_3. On the y-axis as the mole fraction of O_2 ranges from 0 to 1, the mole fraction of NH_2 ranges from 1 to 0.

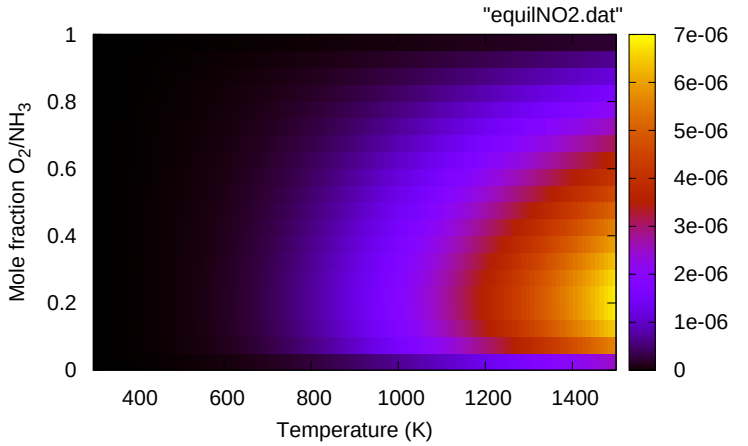

Figure 2: Map of equilibrium composition of NO_2 resulting from a mixture of O_2 and NH_3. On the y-axis as the mole fraction of O_2 ranges from 0 to 1, the mole fraction of NH_2 ranges from 1 to 0.

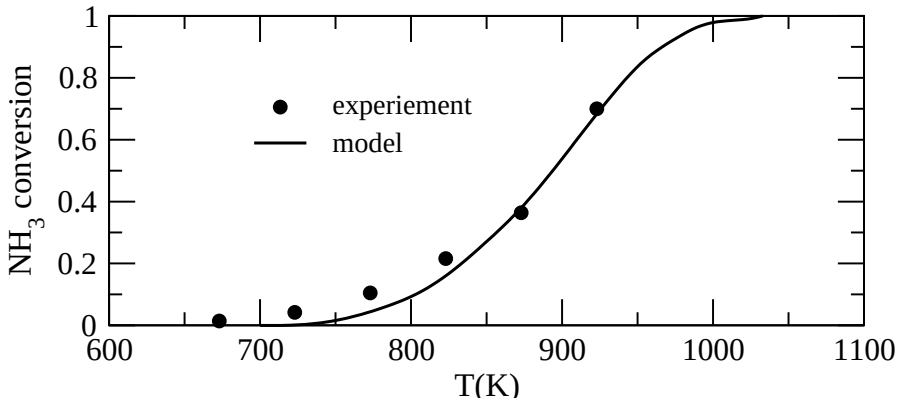

Figure 3: Cor

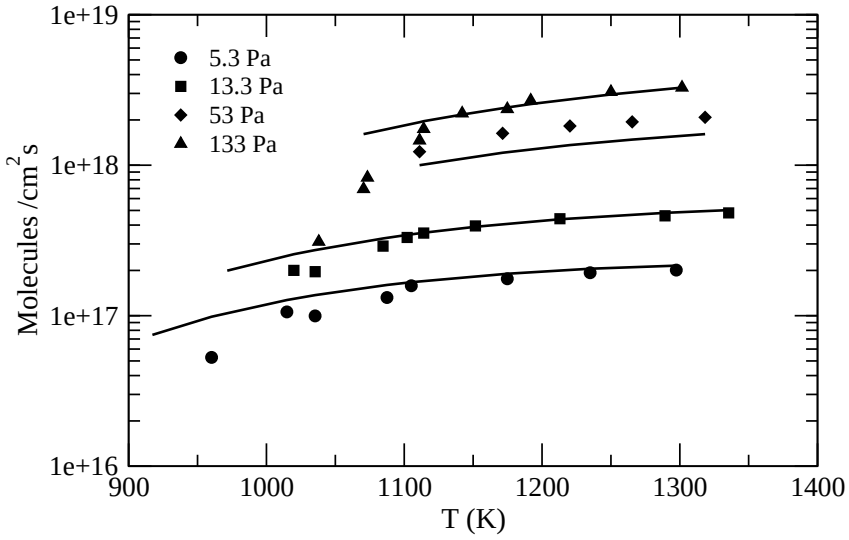

Figure 4: Comparison of e
1983), and the lines stand

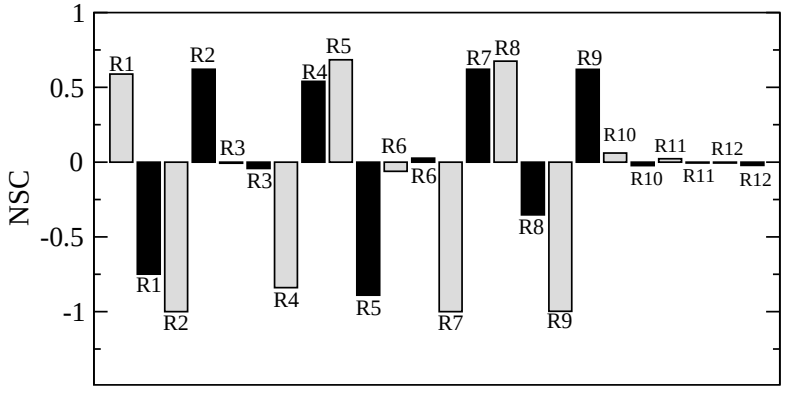

Figure 5: Normalized sensitivity coefficient (NSC) for NH_3 conversion at 1073 K. Black filled boxes indicate a change of +10% in the pre-exponentials or sticking coefficient, and gray filled bars indicate a corresponding -10% change.

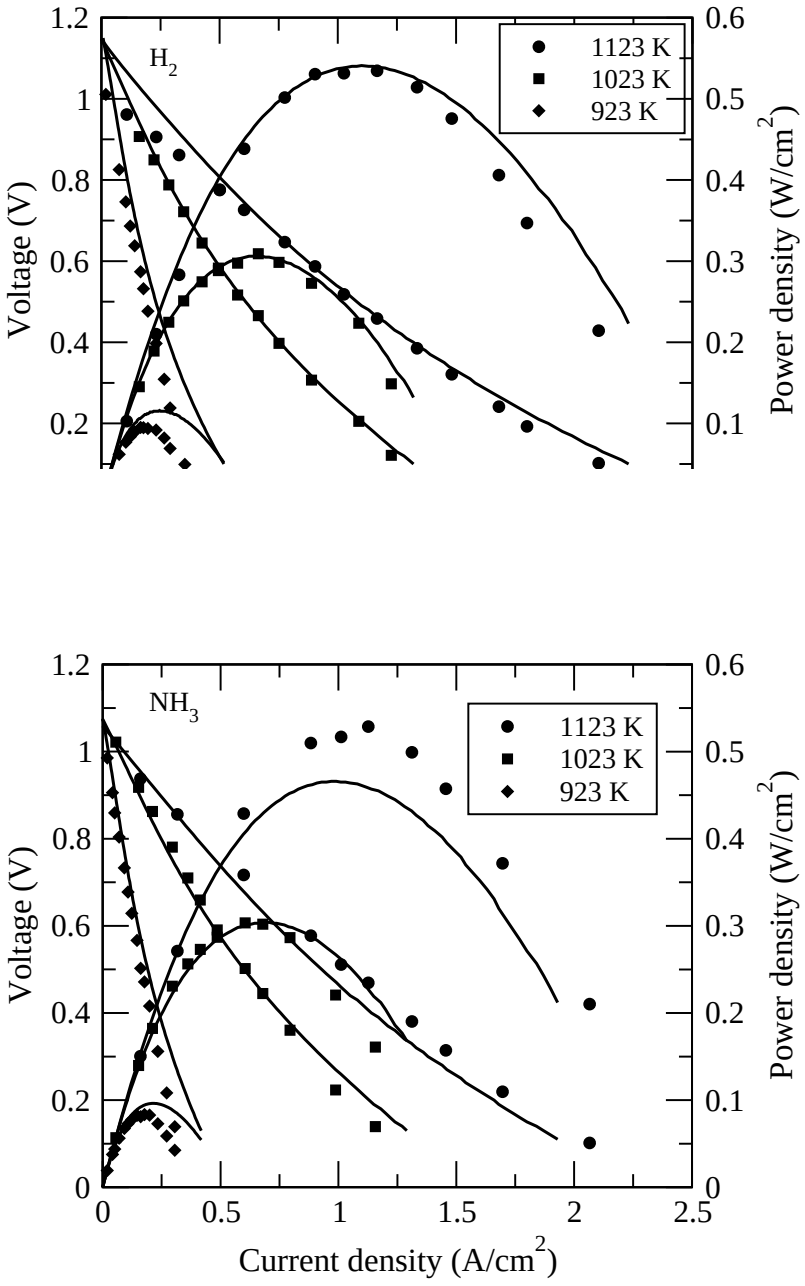

(b)

Figure 6: Comparison between experimentally observed performance curves and the model predictions (Ref Ma et al. (2007)). The symbols indicate experimentally measured values and the solid lines represent model predictions. (a) shows the comparison between the model predictions and experimental observations for H_2 (b) shows the comparison between model predictions and experimental observations for NH_3.

Figure 7: Limiting current predicted by the kinetic model as a function of specific surface area. The horizontal line represents equilibrium

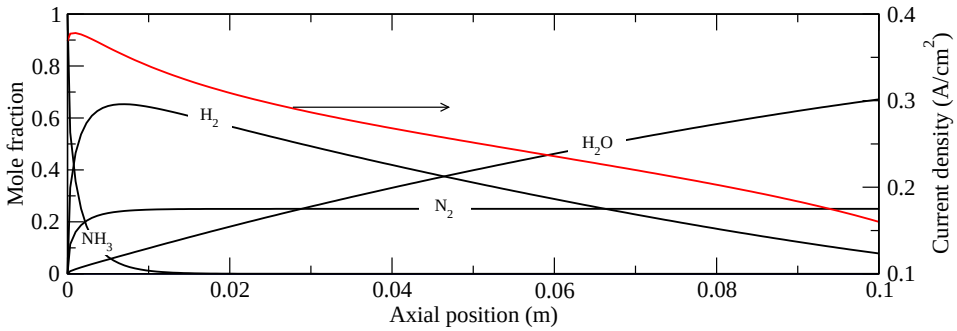

Figure 8: Species profiles in the fuel channel and current density along the length of a 10 cm long planar cell. 100% NH_3 is considered to enter the fuel channel at 0.1 m/s and air at 5 m/s is in the air channel. The MEA parameters used for this calculation is same as the ones given in Table 4